Materials Science & Engineering A 755 (2019) 28–36

Contents lists available at ScienceDirect

Materials Science & Engineering A

journal homepage: www.elsevier.com/locate/msea

Achieving an ultra-high strength in a low alloyed Al alloy via a special structural design

X.H. Zeng[a,b], P. Xue[a,**], L.H. Wu[a,*], D.R. Ni[a], B.L. Xiao[a], Z.Y. Ma[a]

[a] Shenyang National Laboratory for Materials Science, Institute of Metal Research, Chinese Academy of Sciences, 72 Wenhua Road, Shenyang, 110016, China
[b] Technology Center, Zhuzhou CRRC Electric Times Co., Ltd, Zhuzhou, 412001, China

ARTICLE INFO

Keywords:
Aluminum alloys
Ultrafine-grain
Friction stir processing
Aging
Low alloyed high-strength alloys

ABSTRACT

An ultrafine-grained (UFGed) low alloyed aluminum alloy (6061 Al alloy) with a special nano-sized spherical precipitate structure was achieved by friction stir processing (FSP) and post-FSP aging. The evolution of the grains and precipitates during post-FSP aging and their contribution to mechanical properties were investigated. Under a low rotation rate (200 rpm) with water cooling, the average grain size of the FSP sample was only 200 nm. The ultimate tensile strength of the UFG 6061Al alloy aged at 100 °C for 20 min achieved 573 MP with a high elongation of 17%. This strength was nearly 90% higher than that of 6061 Al-T6 alloy (~300 MPa), and was equivalent to that of commercial 7075Al-T651 alloy (~572 MPa, the typical high alloyed Al alloy). Such a good mechanical property was attributed to the good thermal stability and the accelerated precipitation of the FSP UFGed structure under the low-temperature and short-time aging conditions. Further, the contribution of various strengthening mechanisms to the total strength in post-FSP aged Al alloys was quantitatively evaluated. This work provides an effective strategy for obtaining low alloyed high-strength Al alloys, which is beneficial for reducing environmental burdens and improving long-term sustainability.

1. Introduction

Global climatic warming resulting from greenhouse gas emissions, such as CO_2, is an acute environmental issue [1]. Vehicular exhaust is one of the most important sources of greenhouse gases [2]. Recently, lightweight design has been proven to be an effective strategy of decreasing the volume of vehicular exhaust [2]. Thus, lightweight design is the main trend in the automobile industry for reducing greenhouse gases.

It is generally known that using light-weight and high-strength metals is a key technology in lightweight vehicle manufacturing [3,4]. Light metals, such as Al and Mg alloys, are used to achieve the light-weight goal, and alloying elements are usually added to achieve the high-strength [5]. However, alloying makes material development more resource intensive [6]. Meanwhile, alloyed materials with complicated compositions might be also more difficult to recycle. Thus, adding alloying elements might have a negative impact on the long-term sustainability of high-performance metals [6].

To make materials plain, which has been proposed in 2017 [6,7], means that novel properties and performance can be achieved in the "plain" materials with low alloying or even non-alloying via introducing architectural defects across different length-scales. Various defects, such as vacancy, dislocation, grain boundary and phase boundary, widely exist in crystalline solids. These defects directly influence materials' physical, chemical, and mechanical properties [8]. Thus, to introduce architectural defects is an effective strategy of enhancing the mechanical properties of metals without changing chemical compositions.

6xxx series Al alloys, which are the so-called Al-Mg-Si alloys, are known as typical precipitation-hardened alloys [9]. Compared with other precipitation-hardened Al alloys, such as 2xxx series and 7xxx series Al alloys, alloying elemental contents are lower in 6xxx series Al alloys [10]. More importantly, the cost of adding Mg and Si are cheaper than adding other elements. Thus, 6xxx series Al alloy is a good choice for making materials plain, although the strength of this Al alloy is relatively low. For example, a commercial 6061Al alloy obtained by peak aging only exhibits an ultimate tensile strength (UTS) of ~300 MPa.

Metals and alloys can be strengthened by introducing more grain boundaries via grain refinement [11]. Grain refinement induced by plastic strain in metals and alloys is a well-known phenomenon. Thus, various severe plastic deformation (SPD) methods, such as

* Corresponding author. Tel./fax: +86 24 23971749.
** Corresponding author. Tel./fax: +86 24 23971749.
E-mail addresses: pxue@imr.ac.cn (P. Xue), lhwu@imr.ac.cn (L.H. Wu).

https://doi.org/10.1016/j.msea.2019.03.126
Received 16 January 2019; Received in revised form 29 March 2019; Accepted 30 March 2019
Available online 03 April 2019
0921-5093/

Table 1
Strain, strain rate, and minimum grain size of SPD 6xxx series Al alloys or pure Al.

Fabrication method	Strain	Strain rate (s^{-1})	Minimum grain size (nm)	Ref.
ARB	4	< 10	300	[17]
ECAP	8	–	200	[12]
HPT	100	< 25	100	[13]
FSP	35	75	80	[15,18]
SMAT (pure Al)	20–45	~10^3	30	[14,16]

accumulative roll bonding (ARB), equal-channel angular pressing (ECAP), and high-pressure torsion (HPT), friction stir processing (FSP), and surface mechanical attrition treatment (SMAT) [12–19], were developed as effective methods for designing grain size in metals and alloys.

Table 1 shows the strain, strain rate, and minimum grain size in 6xxx series Al alloys or pure Al processed by various SPD technologies [12–18]. It can be found that ultrafined or nanostructured grains can be prepared by these SPD methods [13–16,18]. However, among all these SPD methods, FSP is the only method to fabricate bulk metals with UFGs or nanostructured grains [19,20]. For example, Nakata et al. [19] obtained large processed area with a size of 250 × 56 × 4 mm by multi-pass FSP in an Al-Si-Cu alloy. Therefore, FSP exhibits an incomparable advantage over other SPD methods to produce large-area UFG or nanostructured metals.

As a kind of typical precipitation-hardened Al alloy, precipitation results in the strength increase in 6xxx series Al alloys [21]. However, because of the concomitant grain growth of the ultrafine-grained (UFGed) Al alloys during post-SPD aging [21–23], controlling the grain size in UFG Al alloys during aging is a big challenge. For 6xxx series Al alloys, HPT [13,21], ARB [17], and ECAP [24,25] processes with post-SPD aging only resulted in slight strength enhancement, or even caused a reduction in strength [26]. However, Xue et al. [27] found that unlike other SPD Cu with a big grain coarsening, FSP Cu exhibited a stable UFG structure without grain coarsening after high cycle fatigue tests, which indicated that UFG metals prepared by FSP might be a relatively stable structure. Thus, it is expected to control the grain size of FSP UFG Al alloys during post-FSP aging by selecting proper aging conditions.

In this study, in order to obtain low alloyed high-strength Al alloys, grains were designed at via FSP at the sub-micro scale, while the precipitates were designed via FSP and subsequent post-FSP aging at the nano scale. The microstructural evolution of FSP Al alloys during post-FSP aging was carefully examined. Finally, the contribution of various strengthening mechanisms to the total strength in post-FSP aged Al alloys was quantitatively evaluated.

2. Experimental procedure

Commercial 6061Al alloy plates, 2 mm in thickness and in a T6 aging state, were used in this work as the parent metal (PM). Here, the T6 aging state was chosen as the initial state just because this state of 6061 Al alloy is commonly used in the practical engineering applications. The nominal chemical compositions of PM are listed in Table 2 and the content of the total alloying elements is 2.43 wt%.

The original plates were subjected to FSP along the rolling direction and the tool with a shoulder 10 mm in diameter and a pin 3 mm in root diameter and 1.82 mm in length (taper thread pin) was used in this study. Additional rapid water cooling was used to obtain a low heat input during the FSP process. FSP was conducted at rotation rates of 400 and 200 rpm with a constant traverse speed of 100 mm/min, which were defined as 400-W and 200-W, respectively. Meanwhile, conventional FSP process was also completed in air at 400 rpm with the same traverse speed, and was defined as 400-A for the samples. In order to further improve the mechanical properties, the 200-W sample was artificial aged after FSP. The aging temperatures were from 80 °C to 175 °C.

Table 2
Chemical compositions of 6061Al-T6 sheets (wt.%).

Mg	Si	Fe	Cu	Zn	Al	Total alloying elements
1.08	0.59	0.3	0.21	0.25	bal.	2.43

The cross-sectional FSP samples were machined perpendicular to the processing direction. The macrostructural characterization of FSP samples was investigated using optical microscopy (OM, HC-300Z/OL, Olympus Corporation) and the detailed microstructure of the FSP and post-FSP aged samples were carried out by transmission electron microscopy (TEM, FEI TECNAI G^2 20) combined with energy dispersive spectroscopy (EDS, OXFORD) and scanning transmission electron microscopy (STEM). The grain size was measured by TEM with the linear intercept method. The volume fraction of precipitates was determined by the area of the whole area of the TEM image divided by the area of the precipitates, and the relative volume fraction of precipitates for the post-FSP aged sample was determined by the volume fraction of precipitates for the T6 aging state divided by that for the post-FSP aged samples. 6061 Al alloy in a solid solution state and 200-W sample were analyzed by means of differential scanning calorimetry (DSC). The DSC experiments were carried out under an argon atmosphere using a METTLER-1100LF system between room temperature and 500 °C with a heating rate of 10 °C/min.

Vickers microhardness measurements were performed on the processed zones (PZ) under a load of 50 g for 15 s. Tensile specimens with a gauge length of 2.5 mm were machined in the PZ parallel to the processing direction and the geometry of the tensile specimen is shown in Fig. 1. Tensile tests were carried out at room temperature at an initial strain rate of 1×10^{-3} s^{-1}.

3. Results

3.1. Microstructural characterization and mechanical properties of FSP samples

Fig. 2 shows the cross-sectional macrostructures of FSP samples under various processing conditions. Under the investigated processing parameters, there were no defects, such as cavities and cracks in the FSP samples. Besides, the PZs produced by FSP exhibited basin shapes with wide top regions.

The TEM micrographs and statistical distributions of the grain sizes in the PZs of FSP samples are shown in Fig. 3. UFGs were obtained in all FSP samples (Fig. 3(a), (c), and (e)) and the average grain sizes of the 400-A, 400-W, and 200-W samples were 700, 400, and 200 nm (Fig. 3(b), (d), and (f)), respectively. It is obvious that finer grain sizes were attributed to the decrease of the heat input via the decrease of the rotation rate or additional water cooling methods.

The magnified TEM micrographs of the precipitates in the 400-W and 200-W samples are shown in Fig. 4. Many spherical precipitates

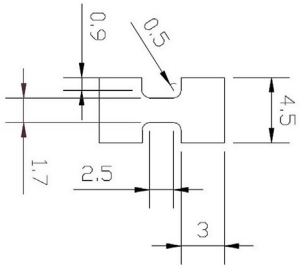

Fig. 1. Geometry of tensile specimens.

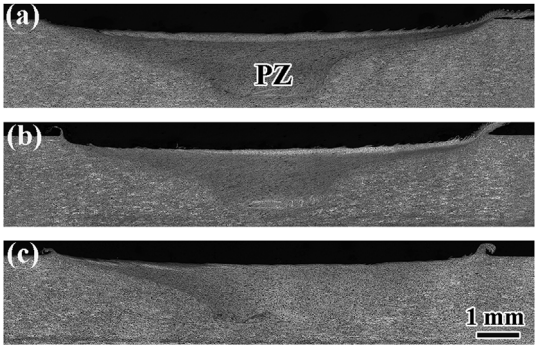

Fig. 2. Macrostructural characterization of FSP 6061 Al alloys: (a) 400-A, (b) 400-W, and (c) 200-W.

with the size of 10–70 nm were found in the 400-W sample (arrow in Fig. 4(a)). However, for the 200-W sample, only few small spherical precipitates were detected, and the average particle size was less than 10 nm (Fig. 4(b)). Thus, the 200-W sample can be approximately considered as an UFG Al alloy in a solid solution state.

The STEM micrographs and EDS mapping of the precipitates in the 400-A sample are shown in Fig. 5. Some large spherical precipitates rich in Fe, Cr, and Mn elements (Points 1 and 2) can be observed in this sample. These spherical precipitates were also obtained in FSP and HPT 6061 Al alloys by Feng et al. [28] and Mohamed et al. [13]. In addition, many light rod-like precipitates only rich in Mg and Si elements were also observed in the 400-A sample (Points 3 and 4). Sauvage et al. [21] reported that these light precipitates in SPD 6xxx series Al alloy were determined to be β phase, depending on the results of Mg/Si ratio and diffraction patterns.

Table 3 shows the microhardness values of the PM and various FSP samples. The PM showed a typical hardness value of 6061 Al alloy in a T6 state, which was 102 HV. The microhardness value of the 400-A sample was only 72 HV, which were smaller than the PM. In comparison, obvious hardening was observed in the 400-W and 200-W samples, and the microhardness values were 113 and 147 HV, respectively.

The engineering stress-strain curves of the PM and all FSP samples are shown in Fig. 6. The ultimate tensile strength (UTS) of 328 MPa were obtained in the PM. Under the condition of 400 rpm and air cooling (the 400-A sample), the UTS were only 232 MPa. Under water cooling, the UTS of the 400-W sample reached up to 376 MPa. The elongation to failure of the 400-W sample was as high as 18.5%, which

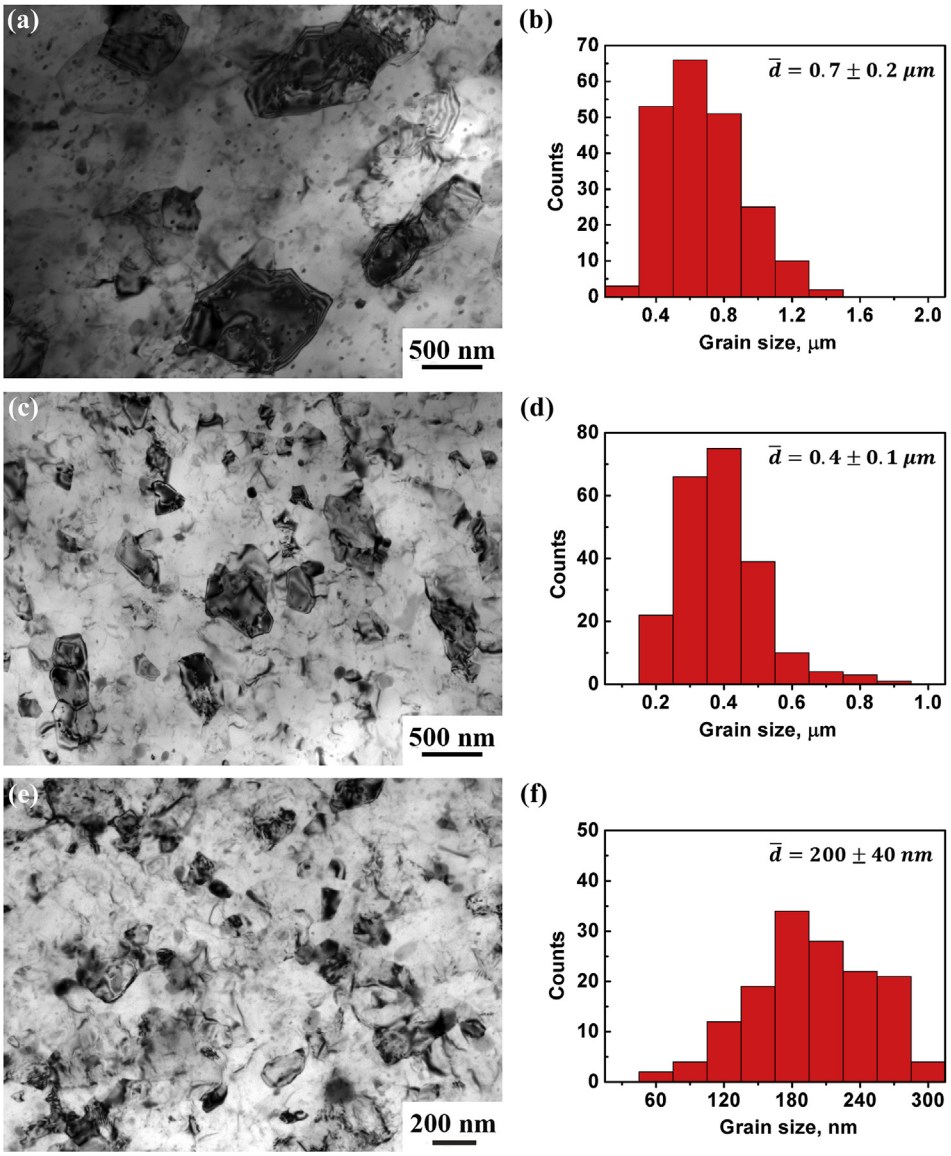

Fig. 3. Grain structures and grain size statistical distributions in PZs of FSP samples: (a) and (b) 400-A, (c) and (d) 400-W, and (e) and (f) 200-W.

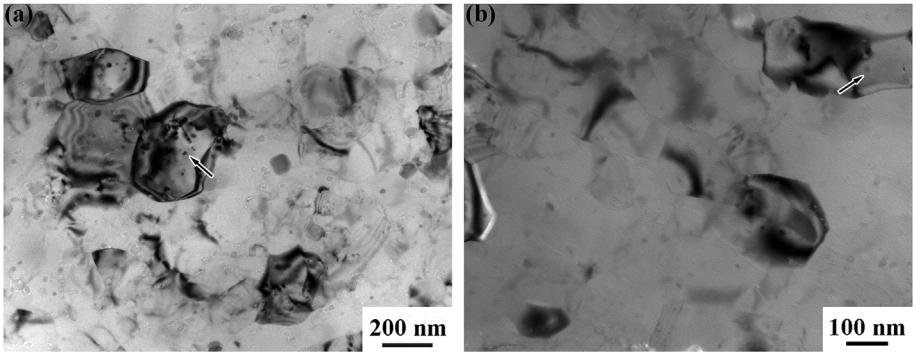

Fig. 4. TEM micrographs of precipitates in (a) 400-W and (b) 200-W samples.

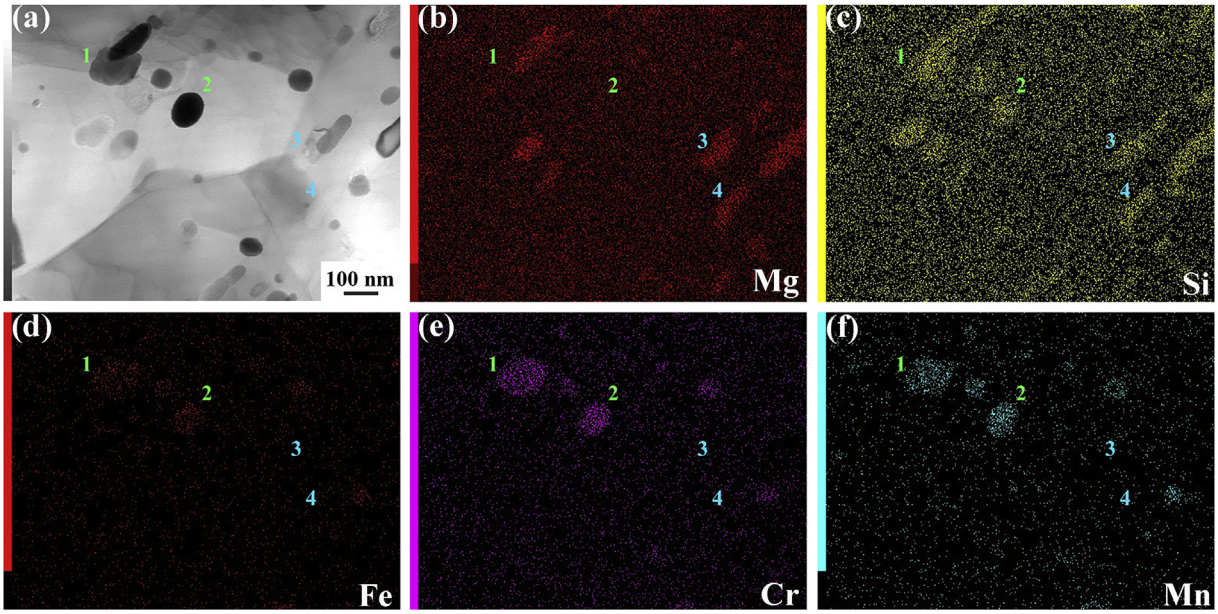

Fig. 5. (a) STEM image and corresponding EDS mappings with (b) Mg, (c) Si, (d) Fe, (e) Cr, and (f) Mn for 400-A sample.

Table 3
The microhardness of PM and various FSP samples.

	PM	400-A	400-W	200-W
Microhardness (HV)	102 ± 3	72 ± 1	113 ± 2	147 ± 4

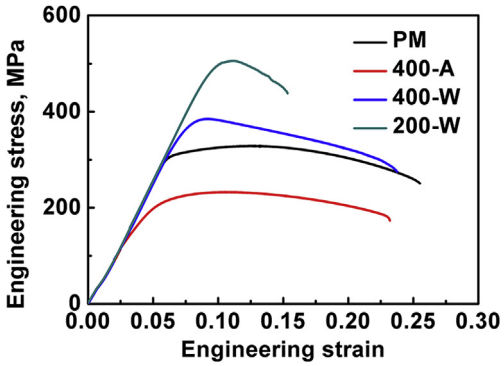

Fig. 6. The engineering stress-strain curves of PM and various FSP samples.

exhibited a similar value of the PM (21.0%). For the 200-W sample, the UTS of 506 MPa was achieved, which was significantly higher than that of the PM.

3.2. Microstructural evolution and mechanical properties during post-FSP aging

From the above results, it was observed that only few precipitates existed in the 200-W sample (Fig. 4(b)), so the strength of this sample can be improved by post-FSP aging. Fig. 7(a) shows the microhardness profiles of 200-W samples after post-FSP aging at different temperatures and time. At the aging temperatures of 80 °C–140 °C, the microhardness rapidly increased to a peak value. Thereafter, the microhardness value decreased with the extension of the aging time. Under the aging conditions of 100 °C and 20 min, the microhardness value was the highest, which reached to a high microhardness level of 161 HV. At a conventional aging temperature of 175 °C, the microhardness value decreased all the time during post-FSP aging.

The engineering stress-strain curves of 200-W samples after post-FSP aged at 100 °C for different durations are shown in Fig. 7(b). Clearly, the 200-W sample after aging 20 min exhibited the highest strength and elongation, with UTS reaching up to 573 MPa, and a surprising high elongation of 17% was obtained. This result was very exciting because this strength was nearly 90% higher than that of 6061 Al-T6 alloy (~300 MPa), and was equivalent to that of commercial 7075Al-T651 alloy (~572 MPa, the typical high alloyed Al alloy).

The grain evolution of the 200-W samples aging at 100 °C with different aging time is shown in Fig. 8. The grain sizes of post-FSP aged samples at different aging time were measured, as depicted in Fig. 8(a). With aging for 20 min, the average grain size just reached to 240 nm

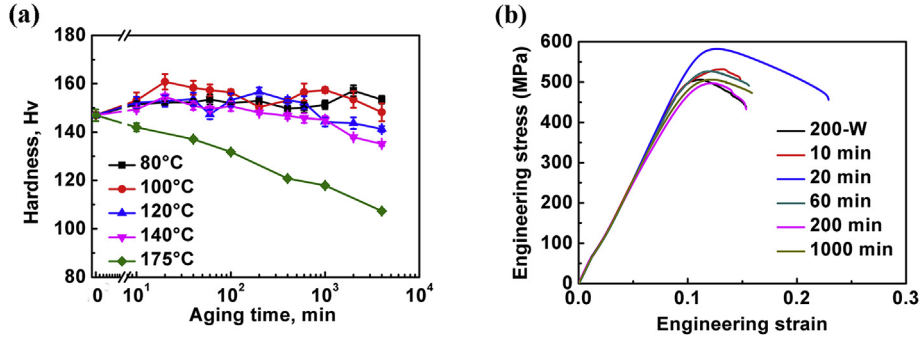

Fig. 7. (a) Variation of microhardness of 200-W samples with post-FSP aging time at different temperatures and (b) engineering stress-strain curves of 200-W samples by post-FSP aging at 100 °C.

(Fig. 8(b)), which was slightly larger than that of the 200-W sample (200 nm). It indicated that the FSP Al-Mg-Si UFG structure exhibited good thermal stability during short-time aging at 100 °C. When the aging time was longer than 200 min, grain growth was observed in the aged samples. It is noticed that although the grain size increased with the aging time increasing during post-FSP aging, the average grain size of all samples were less than 400 nm, which were also in the range of UFG scale.

Generally, the relative volume fraction of the precipitates can be defined as:

$$V_R = \frac{V_S}{V_{T6}} \tag{1}$$

where V_S is the volume fraction of the precipitates in the post-FSP aged sample and V_{T6} is the volume fraction of the precipitates in 6061 Al alloy at a peak aging (T6) state. The relative volume fraction of the precipitates in 200-W samples aging at 100 °C under different aging time is showed in Fig. 9(a). With aging for 20 min, the relative volume fractions of the precipitates increased rapidly and the sizes of most precipitates were less than 10 nm (Fig. 9(b)). With increasing the aging time, both the relative volume fractions and the size of the precipitates continued to increase while the increasing trend decreased (Fig. 9(c), (d), and (e)).

4. Discussion

4.1. Grains and precipitates in FSP and post-FSP aged samples

Various SPD technologies, with high strain and strain rate as well as low temperature have been shown to be beneficial and effective methods of obtaining fine grains [29–31]. Due to the ultra-high strain and strain rate [15,18], FSP is able to realize the grain refining at a low processing temperature. It is well known that decreasing heat input is a key method to reduce the temperature during FSP of Al alloys. Decreasing rotation rate, increasing traverse speed and using additional cooling condition are conventional methods for reducing the heat input during FSP [32–34]. In this study, the average grain size of the 200-W sample (200 nm) was the finest, which was mainly attributed to a very low heat input resulting from the extremely low rotation rate and the additional water cooling condition.

It is well known that the concomitant growth of the UFG occurs in the SPD samples during the aging process, which results in a large decrease of the strength [21]. Thus, selecting an appropriate temperature for controlling grain growth was a critical issue for the UFGs during the aging process. During a conventional peak aging process of 175 °C for 17 h, the microhardness value of post-FSP aged sample (typically with 113 Hv) was much lower than that of 200-W sample (147 Hv). Sauvage et al. [21] also reported that during aging at 170 °C, the

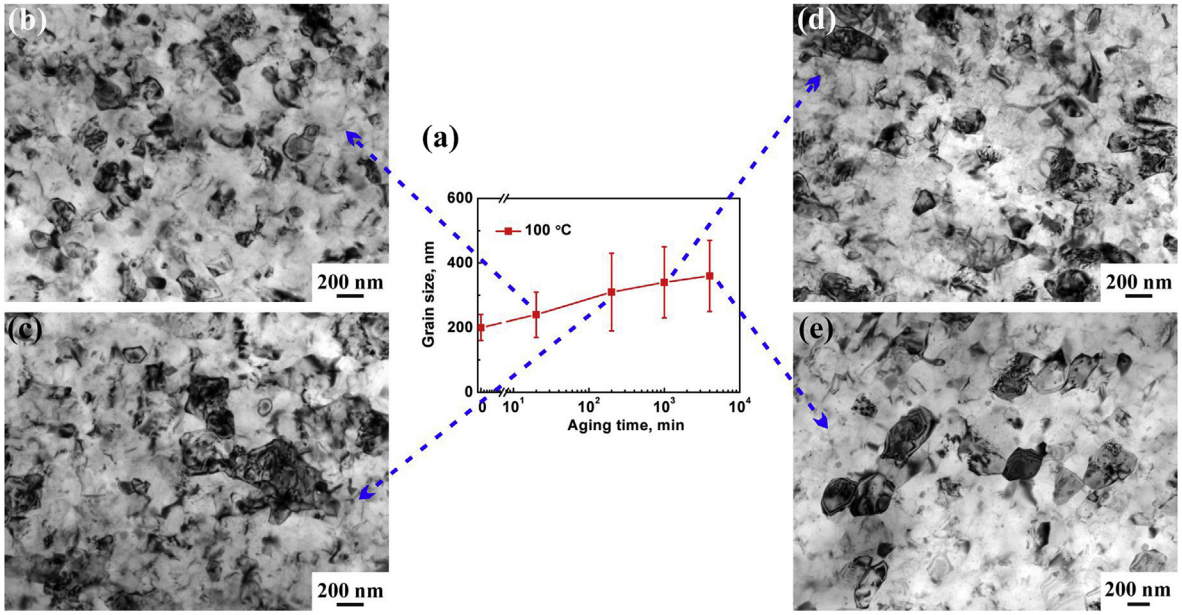

Fig. 8. (a) Variation of grain sizes of 100 °C aged 200-W samples with different aging time. TEM images showing grain structures for aging time of (b) 20, (c) 200, (d) 1000, and (e) 4000 min.

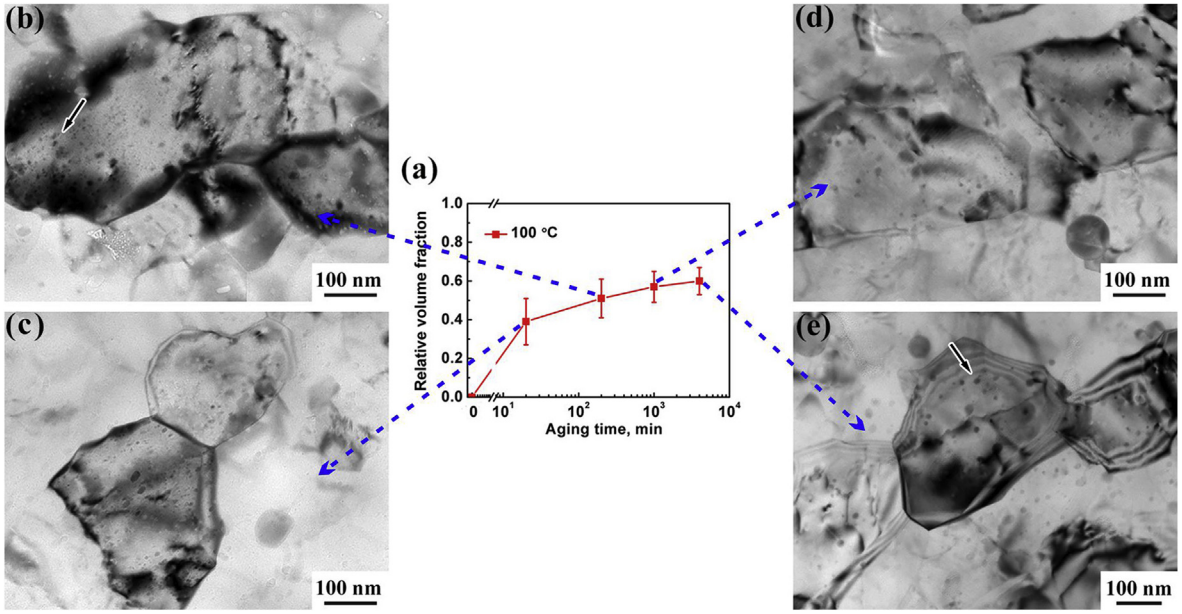

Fig. 9. (a) Relative volume fraction of precipitates in post-FSP aged 200-W samples after different aging times, TEM micrographs of precipitates in samples at (b) 20, (c) 200, (d) 1000, and (e) 4000 min.

grains of HPT UFG sample (the average grain size was about 200 nm) grew to 1000 nm. Meanwhile, for the HPT UFG structure, during aging at a relatively low-temperature (130 °C and 100 °C), the grain size also grew to 600 nm and there was a sharp drop for the hardness during aging [21]. However, in this study, during aging at 100 °C, the average grain size of all FSP samples were less than 400 nm, which indicated that UFG did not experience obvious coarsening during the low-temperature aging process. This might be because that the dynamic recrystallization (DRX) occurs in the FSP of Al alloys, which can release stored energy [18]. Thus, the FSP UFG structure exhibited good thermal stability during short-time aging at 100 °C and the microhardness of FSP sample rapidly increased to a peak (161 Hv) after a short-time.

The DSC curve could analyze the thermal information associated with precipitation of alloys. The DSC curves of the 6061 Al alloy in a solid solution state and the 200-W sample are given in Fig. 10. Usually, there are four exothermic peaks in the DSC curve of A1 base alloy: peak A (~80 °C, GP zones), peak B (~260 °C, β'' precipitates), peak C (~310 °C, β' precipitates), and peak D (~420 °C, β precipitates) [35,36]. However, there was no exothermic peak B in the DSC curve of 200-W sample, which indicated that β'' precipitates were not precipitate during post-FSP aging. Meanwhile, Sauvage et al. [21] reported that according to the results of Mg/Si ratio and diffraction patterns, the precipitates in post-HPT aged 6xxx series Al alloy were only β and β'. Compared with 6061 Al alloy in a solid solution state, 200-W sample had lower GP zones and β' precipitates temperatures, implying an accelerated precipitation rate. The smaller peak area of exothermic peak C also reflected the accelerated precipitation kinetics of 200-W sample.

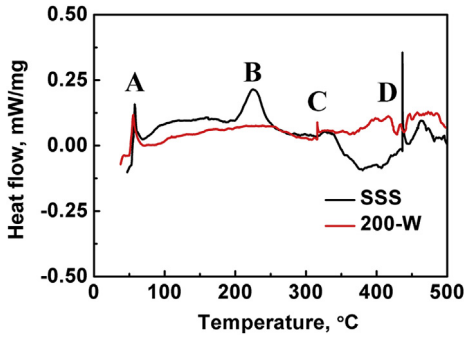

Fig. 10. The DSC curves of 6061 Al alloy in a solid solution state and the 200-W sample.

A mass of defects including vacancies and grain boundaries were generated by plastic deformation during SPD [37,38]. A high density of vacancies were quickly trapped by solute atoms to form clusters after SPD [35], which leaded to lower GP zones and precipitates temperatures and an accelerated precipitation rate. Moreover, grain boundary was a fast channel for element diffusion [33]. The high volume fraction of grain boundaries resulted in the increase of precipitation kinetics. Thus, under the low-temperature and short-time aging conditions, the precipitation of UFG 6061 Al alloy is rapid. Therefore, the high hardness and strength for the aged 200-W FSP sample at 100 °C for 20 min were attributed to the good stability and the accelerated precipitation kinetics of the UFGed structure.

4.2. Relationship between microstructures and properties in post-FSP aged samples

It has been generally accepted that the hardness contribution in a precipitate strengthened alloy of each microstructural characteristics were calculated as follows [13,21]:

$$\mathrm{HV} = HV^{Al} + \Delta HV^{GB} + \Delta HV^{precip} + \sum_i \Delta HV_i^{sol} + \Delta HV^{dislo} \quad (2)$$

where HV^{Al} is the pure Al hardness, which is about 18 HV [39], ΔHV^{GB} is the hardening of grain boundary, ΔHV^{precip} is the hardening of precipitate, and ΔHV_i^{sol} is the solution hardening from the solute i, ΔHV^{dislo} is the strain hardening by dislocations.

Due to the low dislocation density of FSW/FSP grains and poor storage capacity of dislocations in UFGs [40,41], the hardening of dislocation effect can be redlined in this study.

Hall-Petch equation can used to describe the relationship between the hardness (or yield stress) and grain boundary of metals, which can be extended to the SPD Al alloys [13,21]. According to the results of Saito et al. [42], the hardness of a FSP 1050 Al alloy can be written as

$$\mathrm{HV} = 18 + 35d^{-\frac{1}{2}} \quad (3)$$

where d is the grain size. Thus, the grain size contribution is determined to be $\Delta HV^{GB} = 35d^{-\frac{1}{2}}$.

Precipitation strengthening was originated from the precipitate's ability to obstruct the dislocation movement. Assuming that the precipitates are homogeneously distributed, the corresponding yield stress contribution can be written as [43,44]:

$$\Delta\sigma^{precip} = 2M\beta Gb/L \quad (4)$$

where, M is the dimensionless mean orientation factor ($M = 3.06$), β is a constant ($\beta = 0.28$), G is the shear modulus ($G = 26.9$ GPa), b is the burger vector corresponding to (110) dislocations ($b = 0.29$ nm), and L is the average distance between precipitates. For SPD 6xxx series Al alloy, a ratio σ_y/HV is usually determined to 2 [21]. Thus, precipitation hardening is determined to be $\Delta HV^{precip} = 6.68/L$.

Myhr et al. reported that the influence of solute hardening on the yield stress can be written as [44]:

$$\Delta\sigma_i = k_i C_i^{2/3} \quad (5)$$

where $\Delta\sigma_i$ is the absolute increment in yield stress by solute i, C_i is the concentration of solute i, and k_i is the scaling factor for the solute i. The related values for Si and Mg solutes were proposed as follows: $k_{Si} = 66.3$ MPa (wt%) $^{-2/3}$ and $k_{Mg} = 29$ MPa (wt%)$^{-2/3}$ [44].

Usually, for 6xxx series Al alloy with an artificially peak-aged state (T6 state), all alloying elements (Mg and Si) are considered to be precipitated [9]. Thus, the volume fraction of alloying elements in the Al matrix of all post-FSP aged samples can be obtained, according to the precipitate relative volume fraction of post-FSP aged samples (Fig. 9(a)). Then, the solid solution contribution on the hardness can be estimated as: $\Delta HV^{sol} = \Delta\sigma_i/2$ [21].

Based on the above analyses, microhardness profiles of each microstructural feature in the 100 °C aged 200-W samples are shown in Fig. 11(a). Due to the grain growth and the precipitation, the grain boundary hardening and solute hardening decreased, while the microhardness profile of the precipitate hardening increased first and then decreased. Because the precipitation trend of precipitates in UFG 6061 Al alloy was strong, precipitate hardening rapidly increased in a short aging time. Then, with increased aging time, precipitate hardening decreased due to the coarsening of the precipitates. The peak of alloying elements hardening (including precipitate and solute hardening) occurred before precipitates coarsening (1000 min), which was a high microhardness level of 83 HV. With aging for 20 min, the grain boundary hardening, solute hardening, and precipitate hardening of aged FSP sample were 72, 24, and 55 HV, which contributed 45%, 15% and 34% to the total hardness, respectively. Thus, the grain boundary hardening and precipitate hardening are the key reinforcing mechanisms of aged FSP Al alloys, which confirmed that the high strength of post-FSP aged 200-W sample was mainly attributed to the good thermal stability and accelerated precipitate kinetics. Meanwhile, alloying elements hardening of this aged FSP sample reached to 79HV, which was slightly lower than that of 6061Al-T6 (~84 HV).

Following this approach, the measured and estimated microhardness profiles of 100 °C aged 200-W samples are plotted in Fig. 11(b). One can see that the general changing trend for the measured and estimated microhardness profiles show the similar variation trend and the relative difference between the measured and estimated microhardness values did not exceed 5%.

4.3. Low alloyed high-strength Al alloy

The properties of materials are usually determined by their structure. Using the structural and mechanical information presented above, the grain size, microhardness, and microstructure characteristics of the 6061 Al alloy are summarized in Fig. 12. Four regions were differentiated according to structural and mechanical characteristics, as shown in Fig. 12(a). Under the traditional aging process in the commercial 6061 Al alloy plate, the microstructure was characterized by large grains (Fig. 12(d)) and needle-like precipitates (Fig. 12(e)) and the microhardness of this 6061Al-T6 was ~102 HV. When the aging time was too long, the microstructural characteristics were large grains and coarse precipitates and the microhardness was very low (overaging zone in Fig. 12(a)). For the SPD samples, a microstructural characteristic of UFGs exhibited (Fig. 12(c)) and the microhardness could reach up to ~140 HV. By post-SPD aging, the microstructures were characterized by UFGs and spherical precipitates (Fig. 12(b)), with a very high microhardness of 161 HV was achieved in this study. Thus, the combination of SPD and post-SPDed aging was an effective strategy for obtaining a high-strength Al alloy.

The use of materials with low alloying elements is an important and beneficial consideration for reducing environmental burdens and improving long-term sustainability. A comparison of the strengths of Al alloys from different processing technologies and alloying element contents in the present work and previous studies is shown in Fig. 13(a) [13,17,24,26,34,42,45–49]. Most Al alloys exhibit the characteristic of high alloying element content and high strength, with their data points located under a blue curve. Only a data point of Al alloys under the combination process of FSP and post-FSP aging in this study clearly separate from the curve, showing a better comprehensive characteristic including higher strengths and lower element content compared to commercial Al alloys via other processing methods. The UTS of ultrafine-grained low alloyed aluminum alloy reached up to 573 MPa, which were equivalent to those of commercial high alloyed Al alloy (such as 7075Al-T651 alloy, ~572 MPa).

Besides, the UTS of 6061 Al alloys processed by different methods combined with aging in the present work and previous studies is shown in Fig. 13(b). It is obvious that compared to other processing methods and their aged samples, such as HPT/HPT + aging [13,17,24], higher UTS exhibited in the FSP and post-FSP aged samples, which was mainly attributed to the fact that a UFGed structure was obtained by FSP [34], and a good thermal stability and accelerated precipitation of the FSP UFGed structure exhibited when aging at a low-temperature (100 °C) for a short time (20 min). As a result, the UTS of FSP and post-FSP aged

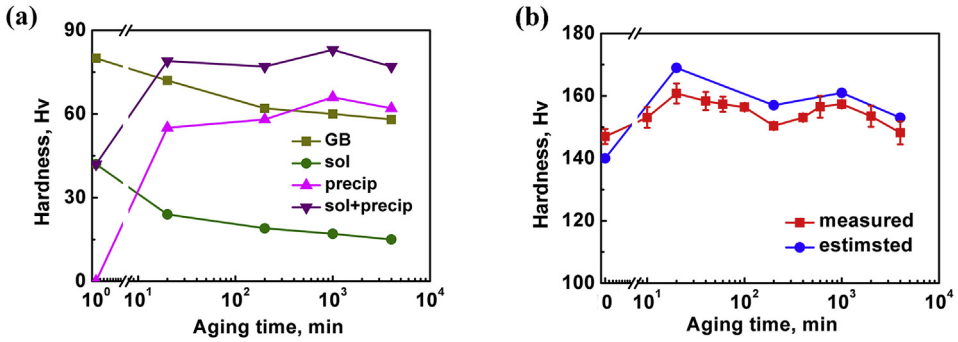

Fig. 11. (a) Microhardness contributions of each microstructural feature in 100 °C aged 200-W samples, (b) measured and estimated microhardness profiles of 100 °C aged 200-W sample.

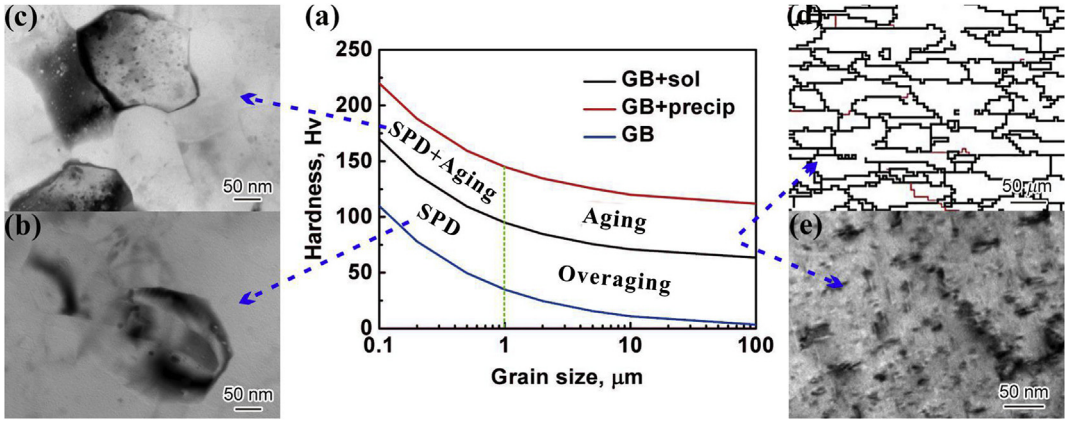

Fig. 12. (a) A map of grain sizes and hardness in 6061 Al alloy; microstructures of (b) post-FSP aging and (c) FSP 6061 Al alloy; and (d) grains and (e) precipitates in 6061 Al alloy in the T6 temper state.

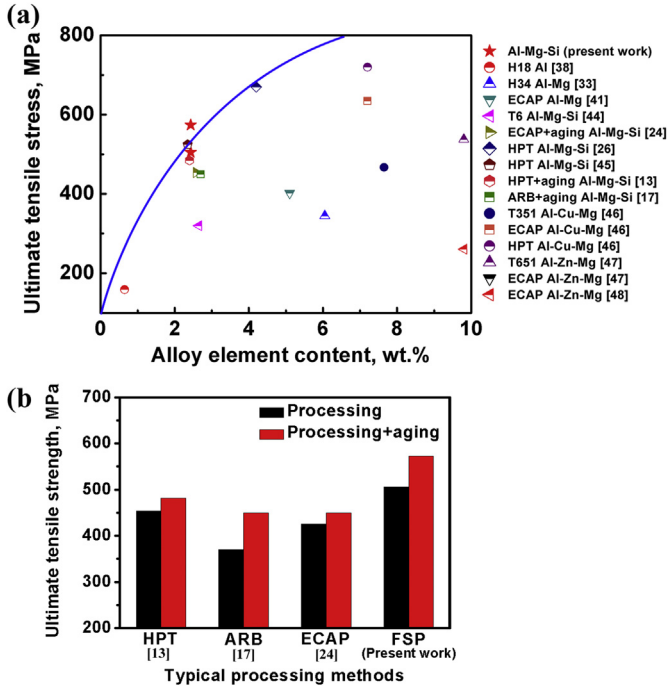

Fig. 13. (a) A comparison of the strength of Al alloys under different processing technologies and alloying element contents, (b) strength of 6061 Al alloy with different processing methods combined with aging.

sample was higher than other processed and post-processing aged 6061 Al alloys [13,17,24]. Therefore, this study provided an effective method for the preparation of low alloyed high-strength Al alloys.

5. Conclusions

A low alloyed high-strength Al alloy was achieved via friction stir processing (FSP) combined with post-FSP aging, and the following conclusions were drawn:

1. The ultrafine grains (200 nm) were obtained at 200 rpm with rapid water cooling. The hardness and UTS of FSP 6061 Al alloy increased with decreased rotation rate and increased cooling rate, which were as high as 147 HV and 506 MPa, respectively, for 200 rpm with rapid water cooling conditions.
2. After post-FSP aging at 100 °C for 20 min, the hardness and UTS of UFG 6061 Al alloy reached up to 161 HV and 573 MPa, respectively, which were nearly 90% higher than those of 6061 Al-T6 alloy, and equivalent to those of the typical commercial high alloyed Al alloy (7075Al-T651 alloy).
3. The high strength for the post-FSP aged UFG 6061 Al alloy was attributed to its good thermal stability and the accelerated precipitation kinetics under the low-temperature and short-time aging conditions.
4. Quantitative evaluation of strengthening mechanisms showed that the grain boundary hardening and precipitate hardening are the key reinforcing mechanisms of aged FSP Al alloys, which contributed 45% and 34% to the total hardness, respectively. The relative difference between the measured and estimated microhardness values did not exceed 5%.

Acknowledgments

This work was supported by the National Natural Science Foundation of China under grant Nos. 51331008, U1508216 and 51301178.

Appendix A. Supplementary data

Supplementary data to this article can be found online at https://doi.org/10.1016/j.msea.2019.03.126.

References

[1] V. Ramanathan, M.V. Ramana, G. Roberts, D. Kim, C. Corrigan, C. Chung, D. Winker, Warming trends in Asia amplified by brown cloud solar absorption, Nature 448 (2007) 575–578.
[2] J.C. Kelly, J.L. Sullivan, A. Burnham, A. Elgowainy, Impacts of vehicle weight reduction via material substitution on life-cycle greenhouse gas emissions, Environ. Sci. Technol. 49 (2015) 12535–12542.
[3] M. Hockauf, M.F.X. Wagner, M. Händel, T. Lampke, S. Siebeck, B. Wielage, High-strength aluminum-based light-weight materials for safety components – recent progress by microstructural refinement and particle reinforcement, Int. J. Mater. Res. 103 (2012) 3–11.
[4] K. Weinert, D. Biermann, S. Bergmann, Machining of high strength light weight Alloys for engine applications, CIRP Ann. 56 (2007) 105–108.
[5] H.M. Lin, S. Kuralay, J.Y. Uan, Microstructural and corrosion characteristics of iron-silicon alloyed layer on 5083 Al alloy by electrical discharge alloying processing, Mater. Trans. 52 (2011) 514–520.
[6] X. Li, K. Lu, Playing with defects in metals, Nat. Mater. 16 (2017) 700–701.
[7] X. Li, L. Yang, K. Lu, Making materials plain: concept, principle and applications, Acta Metall. Sin.
[8] W. Cai, W.D. Nix, Imperfections in Crystalline Solids, Cambridge University Press, London, 2016, p. 1.
[9] S. Esmaeili, D.J. Lloyd, W.J. Poole, Modeling of precipitation hardening for the naturally aged Al-Mg-Si-Cu alloy AA6111, Acta Mater. 51 (2003) 3467–3481.
[10] S.P. Ringer, K. Hono, Microstructural evolution and age hardening in aluminium alloys, Mater. Char. 44 (2000) 101–131.
[11] K. Wang, N.R. Tao, G. Liu, J. Lu, K. Lu, Plastic strain-induced grain refinement at the nanometer scale in copper, Acta Mater. 54 (2006) 5281–5291.
[12] N.V. Thuong, H. Zuhailawati, A.A. Seman, T.D. Huy, B.K. Dhindaw, Microstructural

evolution and wear characteristics of equal channel angular pressing processed semi-solid-cast hypoeutectic aluminum alloys, Mater. Des. 67 (2015) 448–456.
[13] I.F. Mohamed, S. Lee, K. Edalati, Z. Horita, S. Hirosawa, K. Matsuda, D. Terada, Aging behavior of Al 6061 alloy processed by high-pressure torsion and subsequent aging, Metall. Mater. Trans. 46 (2015) 2664–2673.
[14] X.C. Liu, H.W. Zhang, K. Lu, Formation of nano-laminated structure in nickel by means of surface mechanical grinding treatment, Acta Mater. 96 (2015) 24–36.
[15] X.C. Liu, C.S. Wu, G.K. Padhy, Characterization of plastic deformation and material flow in ultrasonic vibration enhanced friction stir welding, Scripta Mater. 102 (2015) 95–98.
[16] H.W. Chang, P.M. Kelly, Y.N. Shi, M.X. Zhang, Thermal stability of nanocrystallized surface produced by surface mechanical attrition treatment in aluminum alloys, Surf. Coating. Technol. 206 (2012) 3970–3980.
[17] M.R. Rezaei, M.R. Toroghinejad, F. Ashrafizadeh, Effects of ARB and aging processes on mechanical properties and microstructure of 6061 aluminum alloy, J. Mater. Process. Technol. 211 (2011) 1184–1190.
[18] L.H. Wu, X.B. Hu, X.X. Zhang, Y.Z. Li, Z.Y. Ma, X.L. Ma, B.L. Xiao, Fabrication of high-quality Ti joint with ultrafine grains using submerged friction stirring technology and its microstructural evolution mechanism, Acta Mater. 166 (2019) 371–385.
[19] K. Nakata, Y.G. Kim, H. Fujii, T. Tsumura, T. Komazaki, Improvement of mechanical properties of aluminum die casting alloy by multi-pass friction stir processing, Mater. Sci. Eng., A 437 (2006) 274–280.
[20] K.J. Al-Fadhalah, A.I. Almazrouee, A.S. Aloraier, Microstructure and mechanical properties of multi-pass friction stir processed aluminum alloy 6063, Mater. Des. 53 (2014) 550–560.
[21] X. Sauvage, E.V. Bobruk, M.Y. Murashkin, Y. Nasedkina, N.A. Enikeev, R.Z. Valiev, Optimization of electrical conductivity and strength combination by structure design at the nanoscale in Al–Mg–Si alloys, Acta Mater. 98 (2015) 355–366.
[22] E. Cerri, P. Leo, Influence of severe plastic deformation on aging of Al–Mg–Si alloys, Mater. Sci. Eng., A 410–411 (2005) 226–229.
[23] A. Deschamps, F. De Geuser, Z. Horita, S. Lee, G. Renou, Precipitation kinetics in a severely plastically deformed 7075 aluminium alloy, Acta Mater. 66 (2014) 105–117.
[24] J.K. Kim, H.G. Jeong, S.I. Hong, Y.S. Kim, W.J. Kim, Effect of aging treatment on heavily deformed microstructure of a 6061 aluminum alloy after equal channel angular pressing, Scripta Mater. 45 (2001) 901–907.
[25] M.Y. Murashkin, I. Sabirov, V.U. Kazykhanov, E.V. Bobruk, A.A. Dubravina, R.Z. Valiev, Enhanced mechanical properties and electrical conductivity in ultrafine-grained Al alloy processed via ECAP-PC, J. Mater. Sci. 48 (2013) 4501–4509.
[26] G. Nurislamova, X. Sauvage, M. Murashkin, R. Islamgaliev, R. Valiev, Nanostructure and related mechanical properties of an Al–Mg–Si alloy processed by severe plastic deformation, Phil. Mag. Lett. 88 (2008) 459–466.
[27] P. Xue, Z. Huang, B. Wang, Y. Tian, W. Wang, B. Xiao, Z. Ma, Intrinsic high cycle fatigue behavior of ultrafine grained pure Cu with stable structure, Sci. China Mater. 59 (2016) 531–537.
[28] A.H. Feng, D.L. Chen, Z.Y. Ma, Microstructure and low-cycle fatigue of a friction-stir-welded 6061 aluminum alloy, Metall. Mater. Trans. 41 (2010) 2626–2641.
[29] Y. Zhang, N.R. Tao, K. Lu, Effects of stacking fault energy, strain rate and temperature on microstructure and strength of nanostructured Cu–Al alloys subjected to plastic deformation, Acta Mater. 59 (2011) 6048–6058.
[30] R. Pippan, F. Wetscher, M. Hafok, A. Vorhauer, I. Sabirov, The limits of refinement by severe plastic deformation, Adv. Eng. Mater. 8 (2006) 1046–1056.
[31] S.Y. Chang, K.S. Lee, S.H. Choi, D. Hyuk Shin, Effect of ECAP on microstructure and mechanical properties of a commercial 6061 Al alloy produced by powder metallurgy, J. Alloy. Comp. 354 (2003) 216–220.
[32] P. Xue, B.L. Xiao, Q. Zhang, Z.Y. Ma, Achieving friction stir welded pure copper joints with nearly equal strength to the parent metal via additional rapid cooling, Scripta Mater. 64 (2011) 1051–1054.
[33] P. Xue, G.M. Xie, B.L. Xiao, Z.Y. Ma, L. Geng, Effect of heat input conditions on microstructure and mechanical properties of friction-stir-welded pure copper, Metall. Mater. Trans. 41 (2010) 2010–2021.
[34] B.B. Wang, F.F. Chen, F. Liu, W.G. Wang, P. Xue, Z.Y. Ma, Enhanced mechanical properties of friction stir welded 5083Al-H19 joints with additional water cooling, J. Mater. Sci. Technol. 33 (2017) 1009–1014.
[35] Y. Weng, Z. Jia, L. Ding, Y. Pan, Y. Liu, Q. Liu, Effect of Ag and Cu additions on natural aging and precipitation hardening behavior in Al-Mg-Si alloys, J. Alloy. Comp. 695 (2017) 2444–2452.
[36] Y. Birol, Restoration of the bake hardening response in a naturally aged twin-roll cast AlMgSi automotive sheet, Scripta Mater. 54 (2006) 2003–2008.
[37] X.C. Liu, H.W. Zhang, K. Lu, Strain-induced ultrahard and ultrastable nanolaminated structure in nickel, Science 342 (2013) 337–340.
[38] B.S. Murty, M.K. Datta, S.K. Pabi, Structure and thermal stability of nanocrystalline materials, Sadhana-Acad. P. Eng. S. 28 (2003) 23–45.
[39] Y.S. Sato, M. Urata, H. Kokawa, K. Ikeda, Hall–Petch relationship in friction stir welds of equal channel angular-pressed aluminium alloys, Mater. Sci. Eng., A 354 (2003) 298–305.
[40] R.S. Mishra, Z.Y. Ma, Friction stir welding and processing, Mater. Sci. Eng. R Rep. R 50 (2005) 1–78.
[41] P. Xue, B.L. Xiao, Z.Y. Ma, High tensile ductility via enhanced strain hardening in ultrafine-grained Cu, Mater. Sci. Eng., A 532 (2012) 106–110.
[42] N. Saito, I. Shigematsu, T. Komaya, T. Tamaki, G. Yamauchi, M. Nakamura, Grain refinement of 1050 aluminum alloy by friction stir processing, J. Mater. Sci. Lett. 20 (2001) 1913–1915.
[43] D. Bardel, M. Perez, D. Nelias, A. Deschamps, C.R. Hutchinson, D. Maisonnette, T. Chaise, J. Garnier, F. Bourlier, Coupled precipitation and yield strength modelling for non-isothermal treatments of a 6061 aluminium alloy, Acta Mater. 62 (2014) 129–140.
[44] O. Myhr, Modelling of the age hardening behaviour of Al–Mg–Si alloys, Acta Mater. 49 (2001) 65–75.
[45] F.C. Liu, Z.Y. Ma, Influence of tool dimension and welding parameters on microstructure and mechanical properties of friction-stir-welded 6061-t651 aluminum alloy, Metall. Mater. Trans. 39 (2008) 2378–2388.
[46] C.M. Cepeda-Jiménez, J.M. García-Infanta, O.A. Ruano, F. Carreño, Mechanical properties at room temperature of an Al–Zn–Mg–Cu alloy processed by equal channel angular pressing, J. Alloy. Comp. 509 (2011) 8649–8656.
[47] E. Khafizova, R. Islamgaliev, Effect of severe plastic deformation on the structure and mechanical properties of Al-Cu-Mg alloy, IOP Conf. Ser. Mater. Sci. Eng. 63 (2014) 012081.
[48] G. Sha, K. Tugcu, X.Z. Liao, P.W. Trimby, M.Y. Murashkin, R.Z. Valiev, S.P. Ringer, Strength, grain refinement and solute nanostructures of an Al–Mg–Si alloy (AA6060) processed by high-pressure torsion, Acta Mater. 63 (2014) 169–179.
[49] G.K. Manjunath, G.V. Preetham Kumar, K. Udaya Bhat, Tensile properties and tensile fracture characteristics of cast Al–Zn–Mg alloys processed by equal channel angular pressing, Trans. Indian Inst. Met. 70 (2017) 833–842.